NANO LETTERS

pubs.acs.org/NanoLett
Letter

Spin States of Trioxotriangulene Controlled by Si−O Bond Formation and Dissociation on $AuSi_x$ Surfaces

Zhangyu Yuan, Toshikaze Kariyado,* Tsuyoshi Murata, Kewei Sun, Donglin Li, Oscar Custance, Yasushi Morita,* and Shigeki Kawai*

Cite This: *Nano Lett.* 2025, 25, 13040−13046

ABSTRACT: The radical molecules have attracted significant attention from researchers because their electronic and spin properties can be controlled via the structure and heteroatoms. With the advancements in on-surface synthesis, it has become possible to conduct spin engineering at the single-molecule level. Here, we investigate the controllable polarized and electronic states of 4,8,12-trioxotriangulene adsorbed on $AuSi_x$/Au(111) surfaces with a combination of scanning tunneling microscopy (STM) operated at 4.3 K and density functional theory calculations. A rich variety of STM topographic contrasts of the molecule reveals various interactions between the molecule and the substrate. We found that the magnetic and electronic properties can be modulated through tip-induced formation and dissociation of a Si−O bond. This finding may pave the way for advancements in molecular spintronics.

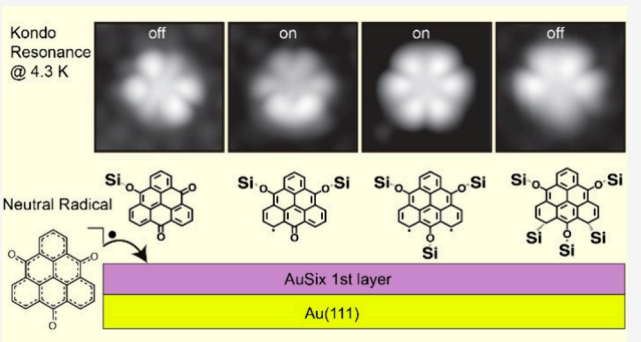

KEYWORDS: *single molecule, neutral radical, spin, Si−O bond, scanning tunneling microscopy, tip-induced manipulation*

Triangulene has attracted tremendous attention from researchers since its first synthesis attempt in 1953.[1] Unlike conventional polycyclic aromatic hydrocarbons, triangulene cannot be drawn with a Kekulé resonance structure. Such open-shell nanographene fragments not only have unique chemical and physical properties[2−8] but also bear great potential for molecular spintronic devices.[9−11] However, the triangulene synthesis in solution is in general challenging due to its high reactivity.[1] Introducing sterically bulky substituents[12,13] is one of the effective methods to obtain stable triangulene radicals in air. However, the bulky groups also reduce the intermolecular interaction, which may hinder the development of their application.[14] By the introduction of three oxo groups, we synthesized and isolated highly air-stable 4,8,12-trioxotriangulene (TOT) without sterically bulky substituents.[15−17] The 3-fold symmetric open-shell 25π-conjugated system is responsible for the high stability due to its delocalized electronic spin distribution with the largest spin density at the central carbon atom. Such properties are crucial for applications in energy conversion and storage,[18,19] spin memories,[20,21] near-infrared absorption,[22] electrical conductors,[23−25] and electrocatalyst for the oxygen reduction reaction.[26] However, it is still unclear how the properties of TOT are modified by substrate adsorption and the chemical bonds at the single-molecule level.

The emergence of an on-surface synthesis strategy, which involves the bottom-up construction of molecular building blocks from small precursor molecules,[27] has realized syntheses of unsubstituted,[28] heterodoped,[29,30] and π-extended[31−33] triangulenes on various surfaces under ultrahigh-vacuum (UHV) conditions. The electronic and magnetic properties were also characterized in detail with scanning tunneling microscopy (STM) at low temperatures.[34−36] Consequently, exotic spin-exchange coupling between the triangulene units has been investigated, in conjunction with successive tip-induced dehydration.[37] Although the high reactivity may lead to further bond formation on the surface, modulating the electronic and magnetic properties of triangulene molecules by chemical bond formation is still scarce.

Here, we study the spin-polarized and electronic states of TOT molecules adsorbed on $AuSi_x$/Au(111) surfaces by low-temperature STM and scanning tunneling spectroscopy (STS). A rich variety of STM topographic contrast of TOT indicates the presence of various interactions between the molecule and the substrate. By applying pulse bias voltages and tip-induced manipulation, we could dissociate the Si−O bond and change

Received: July 4, 2025
Revised: August 9, 2025
Accepted: August 11, 2025
Published: August 13, 2025

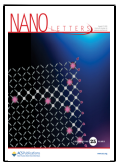

https://doi.org/10.1021/acs.nanolett.5c03477
Nano Lett. 2025, 25, 13040−13046

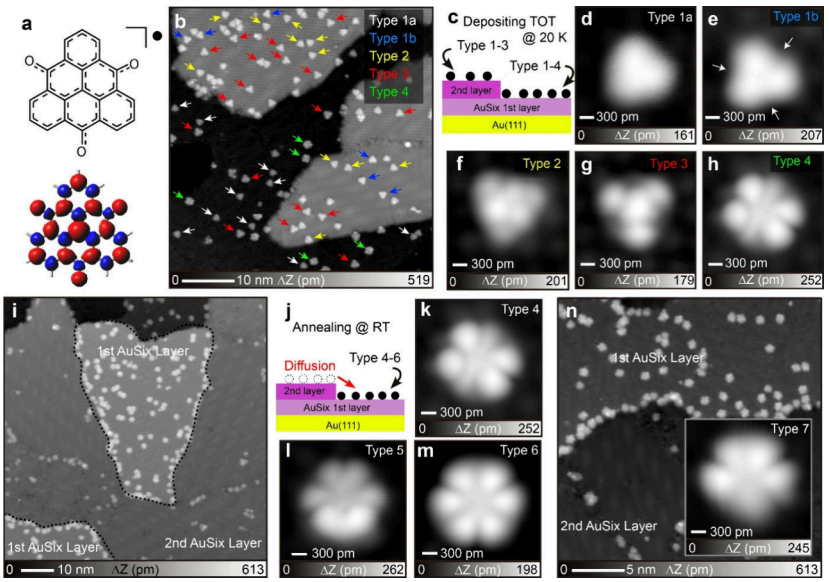

Figure 1. Formation of $AuSi_x$ intercalation and deposition of TOT on $AuSi_x$/Au(111). (a) Chemical structure (upper panel) and electronic spin distribution (lower panel) of TOT. (b) Large-scale STM topography of the sample after deposition of TOT on $AuSi_x$/Au(111) kept at 20 K. Arrows indicate the four different types of TOT. (c) Schematic drawing of the TOT distribution on the first and second $AuSi_x$ layers. Close-up views of type 1 on the first in panel d and second layers in panel e. (f–h) STM topographies of types 2–4 located on the first layer. (i) Large-scale STM topography after annealing the sample at RT for 15 min. The Moiré pattern is seen only on the second $AuSi_x$ layer. (j) Schematic drawing of the sample after annealing at RT. (k–m) Close-view STM topographies of types 4–6 located on the first layer. (n) STM topography of the sample after further annealing at 338 K for 15 min. The inset shows a close-up view of type 7 located on the first layer. Measurement parameters: sample bias V = 200 mV and tunneling current I = 5 pA in panels b, h, k, and l, V = 200 mV and I = 10 pA in panels d, f, g, i, and n, V = 200 mV and I = 100 pA in panel e, and V = 100 mV and I = 50 pA in panel m.

the adsorption site in a controlled manner, resulting in modulations of the electronic and magnetic properties.

The TOT molecules (Figure 1a) were deposited on a $AuSi_x$/Au(111) surface (Figure S1), which was used as an electronic decoupling layer to study the electronic properties of graphene nanoribbons.[38,39] Figure 1b shows the large-scale STM topography taken after the deposition of TOT on $AuSi_x$/Au(111) kept at 20 K. The substrate temperature was low enough so that individual molecules adsorbed homogeneously on both the first and second $AuSi_x$ layers (Figure S2). We identified several types of TOT molecules, named types 1a, 1b, and 2–4, indicated by white, blue, yellow, red, and green arrows, respectively. Among these types, types 1–3 existed on both the first and second layers, whereas type 4 was only seen on the first layer (Figure 1c). To investigate the detailed structures of the TOT, close-up view STM topographies were recorded (Figure 1d–h). Notably, the appearance of type 1 on the first layer differs from that on the second one, which may relate to the different molecule–substrate interactions. Due to this difference in appearance, we further categorized type 1 on the first and second layers into type 1a (Figure 1d) and type 1b (Figure 1e), respectively. More structural contrast in the STM topography of type 1b results from the greater electronic decoupling property of the second layer than that of the first layer (see the arrows in Figure 1e). Types 1–3 (Figure 1d–g) had similar 3-fold symmetryies, while type 4 had a 2-fold symmetry (Figure 1h).

After the sample was annealed at room temperature (RT) for 15 min, most of the molecules on the second layer moved to the first layer, on which the population of the molecule increased, as indicated by black lines (Figure 1i). The thermal diffusion of TOT to the first layer indicates that the molecule–substrate interaction on the second layer is smaller than that on the first one. Only a small amount of "bright dots" remained on the second layer, presumably related to molecules adsorbing at defect sites. Detailed STM images of TOT populations at the first and second layers are shown in Figure S3. Besides the diffusion of the molecule to the first layer (Figure 1j), we have found transformations of type 1–3 molecules to new forms, which are named as types 4–6. Figure 1k–m shows the corresponding close-up views of types 4–6, which no longer have a triangular shape. Figure 1n shows the large-scale STM topography taken after further annealing of the sample at 338 K for 15 min. Type 4–6 molecules eventually transformed into a new form, type 7, with a fish-like shape (inset of Figure 1n). An analysis of the apparent STM corrugations of each type can be found in Figure S4.

Next, STS measurements were conducted. We expected that all types of TOT adsorbed on the $AuSi_x$ layer would have a S = 1/2 open-shell character, which should induce a Kondo resonance near the Fermi level. However, the short-range dI/dV curves measured above types 1–3 had no significant signal, related to the magnetic properties (Figure S5). In contrast, the long-range dI/dV curve of type 1a shows the highest occupied molecular orbital (HOMO) and lowest unoccupied molecular orbital (LUMO) states at −1.07 and 1.67 V, respectively (Figure 2a). Such clear molecular orbital states have been measured for pentacene adsorbed on a thin NaCl film formed on Cu(111),[40] which is well-known as an electronic decoupling layer. A similar decoupling effect was measured for fullerene adsorbed on the $AuSi_x$ first layer formed on Au(111),[41] while the decoupling strength of the $AuSi_x$ first layer was weaker than that of the ultrathin NaCl film. Thus, this spectrum indicates that type 1a was significantly decoupled from the gold substrate by $AuSi_x$ intercalation, resulting in no significant interaction between the net spin of TOT and the

https://doi.org/10.1021/acs.nanolett.5c03477
Nano Lett. 2025, 25, 13040−13046

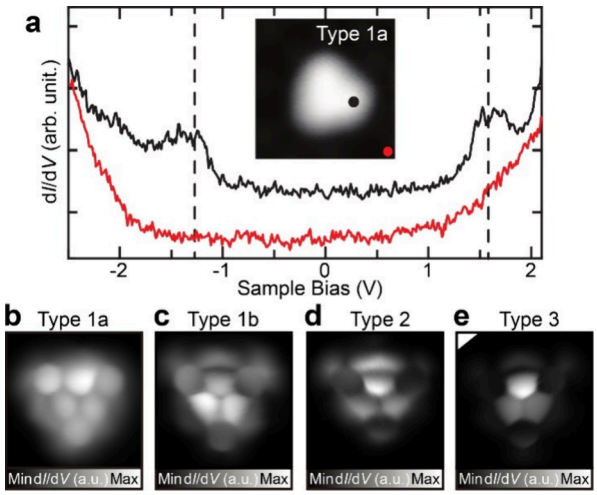

Figure 2. Electronic decoupling and bond-resolved imaging. (a) Long-range dI/dV curve of type 1a located on the first AuSi$_x$ layer. The red curve was taken from the AuSi$_x$ surface as a reference. The curves are shifted vertically for clarity. Set point of the gap: V = 200 mV and I = 100 pA. (b−e) Contant-height high-resolution dI/dV maps taken at V = 1 mV with V_{ac} = 10 mV. Type 1a was located on the first AuSi$_x$ layer, while types 1b, 2, and 3 were located on the second layer.

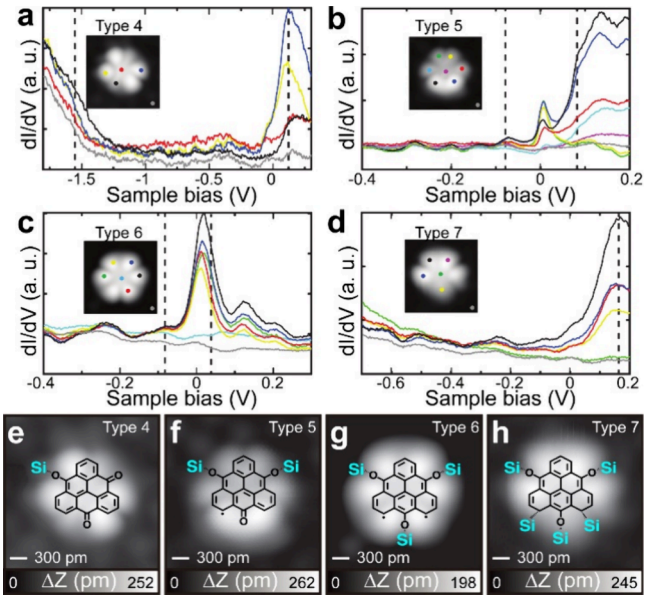

Figure 3. STS and magnetic fingerprints. (a−d) dI/dV curves measured above types 4−7 located on the first AuSi$_x$ layer and (e−h) corresponding proposed chemical structures. Gray curves were taken on the AuSi$_x$ surface as references. Measurement parameters: before each dI/dV curve measurement, the tip−sample gap was adjusted at V = −1.6 V, I = 100 pA, and V_{ac} = 10 mV in panel a, V = −400 mV, I = 100 pA, and V_{ac} = 10 mV in panels b and c, V = −600 mV, I = 100 pA, and V_{ac} = 10 mV in panel d, V = 200 mV and I = 5 pA in panels e and f, V = 100 mV and I = 50 pA in panel g, and V = 200 mV and I = 40 pA in panel h.

conduction electrons of the substrate. We found that the adsorption sites of types 1b, 2, and 3 were frequently changed by applied voltages, which prevented stable long-range STS measurements. To investigate the structures of types 1−3, the tip apex was terminated by a CO molecule.[42] The bond-resolved images show that the TOT molecules were intact, exhibiting the 3-fold symmetric structures and adsorbed flat on the surface (Figure 2b−e). Note that the asymmetric tip effect and tilt of the molecule can be seen in the bond-resolved images.

In contrast to type 1a, distinct peaks appeared in the dI/dV curves taken above types 4−7, which were attributed to HOMO and LUMO as well as the singly occupied molecular orbital and singly unoccupied molecular orbital, as marked by dashed lines (Figure 3a−d). The absence of zero-bias peak indicates the closed-shell structures of types 4 and 7 (Figure 3a and d). In contrast, the dI/dV curves measured above types 5 and 6 have peaks around the Fermi level (Figure 3b and c and Figure S6). The sharp peak of type 5 indicates the existence of a localized unpaired electron spin, characterizing it as a S = 1/2 open-shell structure.[27,33,43−46] In contrast, type 6 had a broadened asymmetric peak, which can be attributed to a S = 1 system.[27,45−49] Two spins are ferromagnetically coupled.[50] We also noticed a peak around 38 mV, indicated by the black dashed line in Figure S6b, which could be related to a molecular orbital. To investigate the presence of Kondo resonance, we conducted temperature-dependent measurements for both types 5 and 6 and found that both curves were broadened with an increasing temperature (Figure S7a and b). However, the temperature dependence of the peak broadening for type 6 was relatively weak. We attempted to fit the measured dI/dV curves with Frota (Kondo peak) and Gaussian (molecular orbital) functions as indicated by purple and blue curves in Figure S7b, respectively. By extracting the effective half width at half maximum (HWHM) values at each temperature (Figure S7c), we obtained a Kondo temperature of 171 K, which is somehow higher than those in previous studies with similar systems.[43−47] We assume that the imperfect peak deconvolution is one of the reasons for such a high Kondo temperature. Nevertheless, types 5 and 6 possess S = 1/2 and 1 characters, respectively. The peaks of the dI/dV curves for both types 5 and 6 were significantly shifted from the Fermi level, and their magnitudes varied, depending on the measurement site on the molecule. We also attribute these shifts to the convolution of molecular orbital signals. The different spin states most likely arose from the bond formations between the oxygen atoms in the TOT molecule and the Si atoms of the substrate (Figure 3f and g). Since type 7 was obtained by higher temperature annealing, we deduced further bond formation between the unpaired electron sites and the Si atoms (Figure 3h). We tentatively assign a structure with one Si−O bond to type 4 (Figure 3e). The corresponding high-resolution images of types 4 and 7 are shown in Figure S8.

Tip-induced manipulation has been employed to reposition molecules[51] and to induce single-molecule reactions,[52−59] which can efficiently induce not only bond formation and dissociation[60] but also configurational switching.[61] We used this technique to prove our proposed chemical structures from an experimental perspective. We first positioned the tip above type 2 on the second AuSi$_x$ layer and set the tip close to the molecule until the tunneling current increased to 6 nA, applying a bias voltage of 200 mV. Then, the tip was laterally moved along the dashed line (Figure 4a). After this manipulation, we found that type 2 was transformed to type 1b. Since the molecule on the first layer was manipulated with a smaller tunneling resistance compared to that on the second layer, we deduce that the interaction between the molecules and the substrate on the first layer is stronger than that on the second layer. Nevertheless, this lateral manipulation reveals

https://doi.org/10.1021/acs.nanolett.5c03477
Nano Lett. 2025, 25, 13040−13046

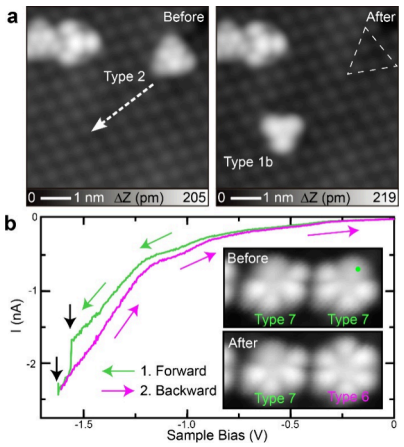

Figure 4. Tip-induced switching of different types of TOT. (a) Switching to type 1b from type 2 located on the second $AuSi_x$ layer by a tip-induced lateral manipulation. (b) Tunneling curve versus sample bias (I−V) curve recorded during a switching event from type 7 to type 6 located on the first layer. Measurement parameters: V = 200 mV and I = 10 pA in panel a.

that the various contrasts found in STM topographies (Figure 1) are related to different adsorption sites on the $AuSi_x$ surface. We could not laterally manipulate types 4−7, which was most likely due to chemical bond formation between the oxo groups and the Si atoms at the surface. Thus, we next attempted to dissociate the bond between the molecule and the silicon atom by exciting the bond with a tunneling current at a given voltage. The tip was positioned above the molecule as indicated by a green dot in the inset of Figure 4b. The bias voltage was swept from 0 to −1.75 V while recording the tunneling current and then swept back to 0 V. After this process, type 7 was switched to type 6. On close inspection of the I−V curve, we found two events indicated by black arrows in Figure 4b, which are most likely related to the dissociation of two C−Si bonds. By repeating the voltage pulses, we were able to dissociate single Si−O bonds one by one and produce types 6, 5, and eventually 4. If the tip-induced manipulations were repeated, we finally obtained an intact TOT, that is, type 1 (Figure S9). This sequential dissociation strongly suggests that type 4 has one Si−O bond. We could also form one Si−O bond, synthesizing type 4 from type 1. However, multiple Si−O bond formation (types 5−7) was unsuccessful, which may be related to the adsorption geometry on the $AuSi_x$ surface.

To understand the detected magnetic properties of TOT on the $AuSi_x$ surface in detail, we conducted density functional theory (DFT) calculations for types 5 and 6 with the generalized gradient approximation (GGA) level using the OpenMX package.[62−64] TOT was first adsorbed on the $AuSi_x$ layer formed on Au(111). Based on the initial position of the molecule, various relaxed structures were obtained. Among them, we found configurations in which two and three oxygen atoms of TOT molecules were connected to Si atoms (Figure 5a and b), namely, types 5 and 6, respectively. As observed in the experiment, type 5 is significantly tilted as the height difference between the highest C atom and the lowest C atom is approximately 70 pm; in contrast, type 6 is almost planar. In both cases, the Si−O bonds induce local deformations in the molecule. Using these relaxed structures, the partial density of states (pDOS) accumulated within the range between the Fermi energy and the bias potential were calculated. The STM topographies of types 5 and 6 were also simulated by

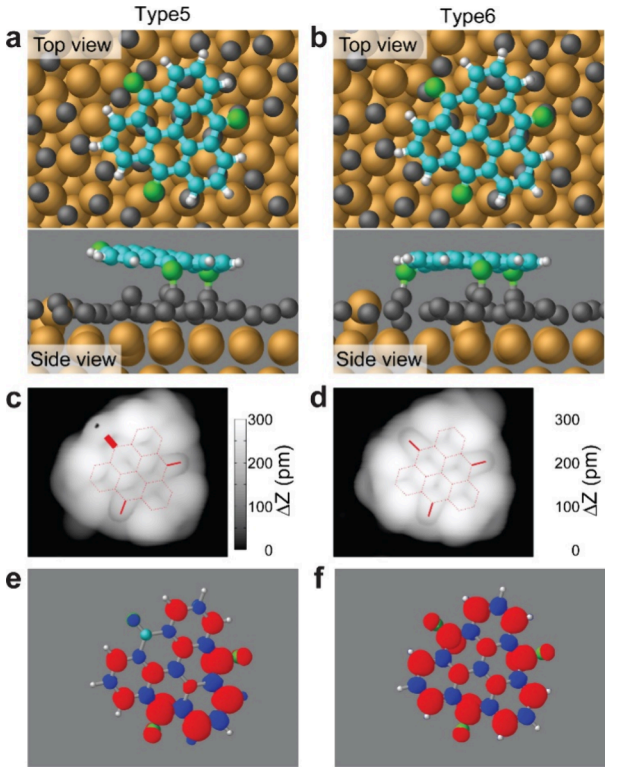

Figure 5. STM contrast and spin density obtained from first-principles calculations. (a and b) Relaxed structures of types 5 and 6 adsorbed on the first $AuSi_x$ layer on Au(111), calculated using DFT with the GGA level: (upper panel) top view and (lower panel) side view. White, cyan, green, gray, and yellow balls represent hydrogen, carbon, oxygen, silicon, and gold atoms, respectively. (c and d) Corresponding simulated STM topographies and (e and f) spin density maps of types 5 and 6. The arrows indicate that the Si atoms are connected to the O atom.

inspecting the shape of the isosurfaces of pDOS, using the Critic2 package (Figure 5c and d).[65,66] We found that the simulated results are in agreement with the experiments. To obtain the spin density distributions, spin GGA calculations were conducted (Figure 5e and f). Clearly, the spin densities resembled those of the isolated molecules corresponding to types 5 and 6. We also calculated the spin density of types 5 and 6 in vacuum at different levels (Figures S10−S13). To represent the Si−O bond, $-SiH_3$ groups were connected to the oxygen atoms of the molecule. We found that the distribution of spin densities for the molecules on the $AuSi_x$ surface and in a vacuum was almost the same, indicating that the $AuSi_x$ substrate has only a marginal effect on the local spin distribution. The calculated spin magnetic moments are ∼0.66 μ_B and ∼1.49 μ_B for types 5 and 6, respectively. The deviation from the values of the isolated molecules (1 and 2 μ_B) most likely results from the weak coupling between the molecular orbitals and the metallic states of the Au slab. Due to the coupling, molecular orbital energies are effectively smeared and partial filling of majority/minority spin states becomes possible. Our Mulliken population analyses indicate that the charge transfers to types 5 and 6 from the surface are 0.38 and 0.50 e, respectively. These excess charges fill the minority spin state, leading to partial cancellation of the spin magnetic moment. We understood that optimizing the Si density in the $AuSi_x$ layer would increase the consistency of the spin magnetic moments; however, due to the high computational

https://doi.org/10.1021/acs.nanolett.5c03477
Nano Lett. 2025, 25, 13040−13046

cost, a thorough investigation of the silicon density is beyond our focus. Nevertheless, our DFT calculations indicate that the formation of the Si−O bond plays a decisive role in the magnetic properties of TOT.

In conclusion, we investigated the spin polarization of TOT on the $AuSi_x$/Au(111) surface and demonstrated that the magnetic and electronic properties can be controlled by the surface and chemical bonding. The rich variety of STM topography contrasts was observed by annealing the sample at different temperatures. We found that the magnetic and electronic properties of the molecule are significantly affected by molecular adsorption sites and the formation of Si−O bonds between the oxo group and the surface silicon atom. We expect that the Si−O bond formation can be achieved using TOT derivatives.[67] Furthermore, these properties can be switched by tip-induced formation and dissociation of the Si−O bonds as well as lateral manipulation of the molecule in a controlled manner. We believe that the ability to control the chemical bonding of radical molecules by the tip may pave the way for advancements in molecular spintronics.

■ ASSOCIATED CONTENT

Supporting Information

The Supporting Information is available free of charge at https://pubs.acs.org/doi/10.1021/acs.nanolett.5c03477.

Detailed experimental sections, detailed theoretical calculation sections, formation of $AuSi_x$/Au(111), as-deposited molecules at 20 K, molecules after annealing at room temperature, line profiles of types 1−7, short-range dI/dV curves of types 1a, 1b, 2, and 3, short-range dI/dV curves of types 4 and 5, temperature dependence of the Kondo peak, high-resolution STM topographies and dI/dV maps of types 4−7, tip-induced switching of different types of TOT, spin density distribution maps calculated in the gas phase, calculation of the radical dianion and diradical trianion, calculation of the triangulene diradical, and line profiles of type 6 (PDF)

■ AUTHOR INFORMATION

Corresponding Authors

Toshikaze Kariyado − *Research Center for Materials Nanoarchitectonics, National Institute for Materials Science, Tsukuba, Ibaraki 305-0044, Japan;* orcid.org/0000-0002-3746-6803; Email: kariyado.toshikaze@nims.go.jp

Yasushi Morita − *Department of Applied Chemistry, Faculty of Engineering, Aichi Institute of Technology, Toyota, Aichi 470-0392, Japan;* orcid.org/0000-0002-2124-0201; Email: moritay@aitech.ac.jp

Shigeki Kawai − *Graduate School of Pure and Applied Sciences, University of Tsukuba, Tsukuba, Ibaraki 305-8571, Japan; Center for Basic Research on Materials, National Institute for Materials Science, Tsukuba, Ibaraki 305-0047, Japan;* orcid.org/0000-0003-2128-0120; Email: kawai.shigeki@nims.go.jp

Authors

Zhangyu Yuan − *Graduate School of Pure and Applied Sciences, University of Tsukuba, Tsukuba, Ibaraki 305-8571, Japan; Center for Basic Research on Materials, National Institute for Materials Science, Tsukuba, Ibaraki 305-0047, Japan;* orcid.org/0000-0001-8028-2893

Tsuyoshi Murata − *Department of Applied Chemistry, Faculty of Engineering, Aichi Institute of Technology, Toyota, Aichi 470-0392, Japan;* orcid.org/0000-0001-6861-5456

Kewei Sun − *Center for Basic Research on Materials, National Institute for Materials Science, Tsukuba, Ibaraki 305-0047, Japan; International Center for Young Scientists, National Institute for Materials Science, Tsukuba, Ibaraki 305-0047, Japan;* orcid.org/0000-0002-1835-243X

Donglin Li − *Center for Basic Research on Materials, National Institute for Materials Science, Tsukuba, Ibaraki 305-0047, Japan*

Oscar Custance − *Center for Basic Research on Materials, National Institute for Materials Science, Tsukuba, Ibaraki 305-0047, Japan;* orcid.org/0000-0001-7931-603X

Complete contact information is available at: https://pubs.acs.org/10.1021/acs.nanolett.5c03477

Notes

The authors declare no competing financial interest.

■ ACKNOWLEDGMENTS

This work was supported in part by the Japan Society for the Promotion of Science (JSPS) KAKENHI Grants 22H00285, 22H02066, 24KF0269, 24K21721, and 25H00422. A part of the calculations in this study was performed on the Numerical Materials Simulator at National Institute for Materials Science (NIMS) and the facilities of the Supercomputer Center, the Institute for Solid State Physics, and The University of Tokyo.

■ REFERENCES

(1) Clar, E.; Stewart, D. G. Aromatic Hydrocarbons. LXV. Triangulene Derivatives. *J. Am. Chem. Soc.* **1953**, *75*, 2667−2672.

(2) Du, J.; Pei, S.; Ma, L.; Cheng, H.-M. 25th Anniversary Article: Carbon Nanotube- and Graphene- Based Transparent Conductive Films for Optoelectronic Devices. *Adv. Mater.* **2014**, *26*, 1958−1991.

(3) Bonaccorso, F.; Sun, Z.; Hasan, T.; Ferrari, A. C. Graphene Photonics and Optoelectronics. *Nat. Photonics* **2010**, *4*, 611−622.

(4) Weiss, N. O.; Zhou, H.; Liao, L.; Liu, Y.; Jiang, S.; Huang, Y.; Duan, X. Graphene: An Emerging Electronic Material. *Adv. Mater.* **2012**, *24*, 5782−5825.

(5) Mak, K. F.; Ju, L.; Wang, F.; Heinz, T. F. Optical Spectroscopy of Graphene: From the sFar Infrared to the Ultraviolet. *Solid State Commun.* **2012**, *152*, 1341−1349.

(6) Nair, R. R.; Blake, P.; Grigorenko, A. N.; Novoselov, K. S.; Booth, T. J.; Stauber, T.; Peres, N. M. R.; Geim, A. K. Fine Structure Constant Defines Visual Transparency of Graphene. *Science* **2008**, *320*, 1308−1308.

(7) Liu, C.-H.; Chang, Y.-C.; Norris, T. B.; Zhong, Z. Graphene Photodetectors with Ultra-Broadband and High Responsivity at Room Temperature. *Nat. Nanotechnol.* **2014**, *9*, 273−278.

(8) Mueller, T.; Xia, F. N. A.; Avouris, P. Graphene Photodetectors for High-Speed Optical Communications. *Nat. Photonics* **2010**, *4*, 297−301.

(9) Morita, Y.; Suzuki, S.; Sato, K.; Takui, T. Synthetic Organic Spin Chemistry for Structurally Well-Defined Open-Shell Graphene Fragments. *Nat. Chem.* **2011**, *3*, 197−204.

(10) Wang, W. L.; Yazyev, O. V.; Meng, S.; Kaxiras, E. Topological Frustration in Graphene Nanoflakes: Magnetic Order and Spin Logic Devices. *Phys. Rev. Lett.* **2009**, *102*, No. 157201.

(11) Han, W.; Kawakami, R. K.; Gmitra, M.; Fabian, J. Graphene Spintronics. *Nat. Nanotechnol.* **2014**, *9*, 794−807.

(12) Inoue, J.; Fukui, K.; Kubo, T.; Nakazawa, S.; Sato, K.; Shiomi, D.; Morita, Y.; Yamamoto, K.; Takui, T. K.; Nakasuji, K. The First Detection of a Clar's Hydrocarbon, 2,6,10-Tri-*tert*-Butyltriangulene: A

Ground-State Triplet of Non-Kekulé Polynuclear Benzenoid Hydrocarbon. *J. Am. Chem. Soc.* **2001**, *123*, 12702−12703.
(13) Arikawa, S.; Shimizu, A.; Shiomi, D.; Sato, K.; Shintani, R. Synthesis and Isolation of a Kinetically Stabilized Crystalline Triangulene. *J. Am. Chem. Soc.* **2021**, *143*, 19599−19605.
(14) Tang, B.; Zhao, J.; Xu, J.-F.; Zhang, X. Tuning the Stability of Organic Radicals: from Covalent Approaches to Non-Covalent Approaches. *Chem. Sci.* **2020**, *11*, 1192−1204.
(15) Morita, Y.; Nishida, S.; Murata, T.; Moriguchi, M.; Ueda, A.; Satoh, M.; Arifuku, K.; Sato, K.; Takui, T. Organic Tailored Batteries Materials Using Stable Open-Shell Molecules with Degenerate Frontier Orbitals. *Nat. Mater.* **2011**, *10*, 947−951.
(16) Morita, Y.; Murata, T.; Ueda, A.; Yamada, C.; Kanzaki, Y.; Shiomi, D.; Sato, K.; Takui, T. Trioxotriangulene: Air- and Thermally Stable Organic Carbon-Centered Neutral π-Radical without Steric Protection. *Bull. Chem. Soc. Jpn.* **2018**, *91*, 922−931.
(17) Ito, H.; Murata, T.; Miyata, T.; Morita, M.; Tsuji, R.; Morita, Y. Air-Stable Thin Films with High and Anisotropic Electrical Conductivities Composed of a Carbon-Centered Neutral π-Radical. *ACS Omega* **2019**, *4*, 17569−17575.
(18) Ito, H.; Murata, T.; Fujisaki, M.; Tsuji, R.; Morita, Y. High Capacity and Energy Density Organic Lithium-Ion Battery Based on Buckypaper with Stable π-Radical. *ChemSusChem* **2021**, *14*, 1377−1387.
(19) Murata, T.; Nakanishi, S.; Nakayama, H.; Ito, H.; Morita, M.; Tsuji, R.; Morita, Y. Rechargeable Batteries with 100% Cathode Active Materials—Conductive Vapor-Deposited Films of a Stable Organic Neutral Radical. *ACS Appl. Energy Mater.* **2022**, *5*, 1218−1225.
(20) Simão, C.; Mas-Torrent, M.; Crivillers, N.; Lloveras, V.; Artés, J. M.; Gorostiza, P.; Veciana, J.; Rovira, C. A Robust Molecular Platform for Non-Volatile Memory Devices with Optical and Magnetic Responses. *Nat. Chem.* **2011**, *3*, 359−364.
(21) Raman, K. V.; Kamerbeek, A. M.; Mukherjee, A.; Atodiresei, N.; Sen, T. K.; Lazić, P.; Caciuc, V.; Michel, R.; Stalke, D.; Mandal, S. K.; Blügel, S.; Münzenberg, M.; Moodera, J. S. Interface-Engineered Templates for Molecular Spin Memory Devices. *Nature* **2013**, *493*, 509−513.
(22) Ikabata, Y.; Wang, Q.; Yoshikawa, T.; Ueda, A.; Murata, T.; Kariyazono, K.; Moriguchi, M.; Okamoto, H.; Morita, Y.; Nakai, H. Near-Infrared Absorption of π-Stacking Columns Composed of Trioxotriangulene Neutral Radicals. *npj Quantum Mater.* **2017**, *2*, 27.
(23) Haddon, R. C. Design of Organic Metals and Superconductors. *Nature* **1975**, *256*, 394−396.
(24) Bryan, C. D.; Cordes, A. W.; Fleming, R. M.; George, N. A.; Glarum, S. H.; Haddon, R. C.; Oakley, R. T.; Palstra, T. T. M.; Perel, A. S.; Schneemeyer, L. F.; Waszczak, J. V. Conducting Charge-Transfer Salts Based on Neutral π-Radicals. *Nature* **1993**, *365*, 821−823.
(25) Murata, T.; Yamada, C.; Furukawa, K.; Morita, Y. Mixed Valence Salts Based on Carbon-Centered Neutral Radical Crystals. *Commun. Chem.* **2018**, *1*, 47.
(26) Murata, T.; Kotsuki, K.; Murayama, H.; Tsuji, R.; Morita, Y. Metal-Free Electrocatalysts for Oxygen Reduction Reaction Based on Trioxotriangulene. *Commun. Chem.* **2019**, *2*, 46.
(27) Clair, G.; de Oteyza, D. G. Controlling a Chemical Coupling Reaction on a Surface: Tools and Strategies for On-Surface Synthesis. *Chem. Rev.* **2019**, *119*, 4717−4776.
(28) Pavlicek, N.; Mistry, A.; Majzik, Z.; Moll, N.; Meyer, G.; Fox, D. J.; Gross, L. Synthesis and Characterization of Triangulene. *Nat. Nanotechnol.* **2017**, *12*, 308−311.
(29) Wang, T.; Berdonces-Layunta, A.; Friedrich, N.; Vilas-Varela, M.; Calupitan, J. P.; Pascual, J. I.; Peña, D.; Casanova, D.; Corso, M.; de Oteyza, D. G. Aza-Triangulene: On-Surface Synthesis and Electronic and Magnetic Properties. *J. Am. Chem. Soc.* **2022**, *144*, 4522−4529.
(30) Li, D.; Silveira, O. J.; Matsuda, T.; Hayashi, H.; Maeda, H.; Foster, A. S.; Kawai, S. On-surface Synthesis of Triaza[5]triangulene through Cyclodehydrogenation and its Magnetism. *Angew. Chem., Int. Ed.* **2024**, *63*, No. e202411893.
(31) Mishra, S.; Beyer, D.; Eimre, K.; Liu, J. Z.; Berger, R.; Groning, O.; Pignedoli, C. A.; Mullen, K.; Fasel, R.; Feng, X. L.; Ruffieux, P. Synthesis and Characterization of π-Extended Triangulene. *J. Am. Chem. Soc.* **2019**, *141*, 10621−10625.
(32) Su, J.; Telychko, M.; Hu, P.; Macam, G.; Mutombo, P.; Zhang, H.; Bao, Y.; Cheng, F.; Huang, Z.-Q.; Qiu, Z.; Tan, S. J. R.; Lin, H.; Jelinek, P.; Chuang, F.-C.; Wu, J.; Lu, J. Atomically Precise Bottom-Up Synthesis of π-extended [5]Triangulene. *Sci. Adv.* **2019**, *5*, No. eaav7717.
(33) Mishra, S.; Xu, K.; Eimre, K.; Komber, H.; Ma, J.; Pignedoli, C. A.; Fasel, R.; Feng, X. L.; Ruffieux, P. Synthesis and Characterization of [7]Triangulene. *Nanoscale* **2021**, *13*, 1624−1628.
(34) Hieulle, J.; Castro, S.; Friedrich, N.; Vegliante, A.; Lara, F. R.; Sanz, S.; Rey, D.; Corso, M.; Frederiksen, T.; Pascual, J. I.; Peña, D. On-Surface Synthesis and Collective Spin Excitations of a Triangulene-Based Nanostar. *Angew. Chem., Int. Ed.* **2021**, *60*, 25224−25229.
(35) Mishra, S.; Catarina, G.; Wu, F.; Ortiz, R.; Jacob, D.; Eimre, K.; Ma, J.; Pignedoli, C. A.; Feng, X.; Ruffieux, P.; Fernández-Rossier, J.; Fasel, R. Observation of Fractional Edge Excitations in Nanographene Spin Chains. *Nature* **2021**, *598*, 287−292.
(36) Mishra, S.; Beyer, D.; Eimre, K.; Ortiz, R.; Fernández-Rossier, J.; Berger, R.; Gröning, O.; Pignedoli, C. A.; Fasel, R.; Feng, X.; Ruffieux, P. Collective All-Carbon Magnetism in Triangulene Dimers. *Angew. Chem., Int. Ed.* **2020**, *59*, 12041−12047.
(37) Yuan, Z.; Zhang, X. Y.; Jiang, Y.; Qian, X.; Wang, Y.; Liu, Y.; Liu, L.; Liu, X.; Guan, D.; Li, Y.; Zheng, H.; Liu, C. L.; Jia, J.; Qin, M.; Liu, P.; Li, D.; Wang, S. Atomic-scale Imaging of Fractional Spinon Quasiparticles in Open-shell Triangulene Spin-1/2 chains. *J. Am. Chem. Soc.* **2025**, *147*, 5004−5010.
(38) Deniz, O.; Sanchez-Sanchez, C.; Dumslaff, T.; Feng, X.; Narita, A.; Müllen, K.; Kharche, N.; Meunier, V.; Fasel, R.; Ruffieux, P. Revealing the Electronic Structure of Silicon Intercalated Armchair Graphene Nanoribbons by Scanning Tunneling Spectroscopy. *Nano Lett.* **2017**, *17*, 2197−2203.
(39) Sun, K.; Silveira, O. J.; Saito, S.; Sagisaka, K.; Yamaguchi, S.; Foster, A. S.; Kawai, S. Manipulation of Spin Polarization in Boron-Substituted Graphene Nanoribbons. *ACS Nano* **2022**, *16*, 11244−11250.
(40) Repp, J.; Meyer, G.; Stojković, S. M.; Gourdon, A.; Joachim, C. Molecules on Insulating Films: Scanning-Tunneling Microscopy Imaging of Individual Molecular Orbitals. *Phys. Rev. Lett.* **2005**, *94*, No. 026803.
(41) Sun, K.; Kawai, S. Strength of electronic decoupling of fullerene on an $AuSi_x$ layer formed on Au(111). *Phys. Chem. Chem. Phys.* **2021**, *23*, 5455.
(42) Gross, L.; Mohn, F.; Moll, N.; Liljeroth, P.; Meyer, G. The Chemical Structure of a Molecule Resolved by Atomic Force Microscopy. *Science* **2009**, *325*, 1110−1114.
(43) Li, J. C.; Sanz, S.; Corso, M.; Choi, D. J.; Peña, D.; Frederiksen, T.; Pascual, J. I. Single Spin Localization and Manipulation in Graphene Open-Shell Nanostructures. *Nat. Commun.* **2019**, *10*, 200.
(44) Sun, Q.; Mateo, L. M.; Robles, R.; Lorente, N.; Ruffieux, P.; Bottari, G.; Torres, T.; Fasel, R. Bottom-up Fabrication and Atomic-Scale Characterization of Triply Linked, Laterally π-Extended Porphyrin Nanotapes. *Angew. Chem.; Int. Ed.* **2021**, *60*, 16208−16214.
(45) Li, J.; Sanz, S.; Castro-Esteban, J.; Vilas-Varela, M.; Friedrich, N.; Frederiksen, T.; Peña, D.; Pascual, J. I. Uncovering the Triplet Ground State of Triangular Graphene Nanoflakes Engineered with Atomic Precision on a Metal Surface. *Phys. Rev. Lett.* **2020**, *124*, No. 177201.
(46) Turco, E.; Bernhardt, A.; Krane, N.; Valenta, L.; Fasel, R.; Juríček, M.; Ruffieux, P. Observation of the Magnetic Ground State of the Two Smallest Triangular Nanographenes. *JACS Au* **2023**, *3*, 1358−1364.
(47) Wang, T.; Sanz, S.; Castro-Esteban, J.; Lawrence, J.; Berdonces-Layunta, A.; Mohammed, M. S. G.; Vilas-Varela, M.; Corso, M.; Peña,

https://doi.org/10.1021/acs.nanolett.5c03477
Nano Lett. 2025, 25, 13040−13046

D.; Frederiksen, T.; de Oteyza, D. G. Magnetic Interactions between Radical Pairs in Chiral Graphene Nanoribbons. *Nano Lett.* **2022**, *22*, 164−171.
(48) Zhu, G.; Jiang, Y.; Wang, Y.; Wang, B.-X.; Zheng, Y.; Liu, Y.; Kang, L.-X.; Li, Z.; Guan, D.; Li, Y.; Zheng, H.; Liu, C.; Jia, J.; Lin, T.; Liu, P.-N.; Li, D.-Y.; Wang, S. Collective Quantum Magnetism in Nitrogen-Doped Nanographenes. *J. Am. Chem. Soc.* **2023**, *145*, 7136−7146.
(49) Su, X.; Li, C.; Du, Q.; Tao, K.; Wang, S.; Yu, P. Atomically Precise Synthesis and Characterization of Heptauthrene with Triplet Ground State. *Nano Lett.* **2020**, *20*, 6859−6864.
(50) Kondo, J. Resistance Minimum in Dilute Magnetic Alloys. *Prog. Theor. Phys.* **1964**, *32*, 37−49.
(51) Kawai, S.; Benassi, A.; Gnecco, E.; Söde, H.; Pawlak, R.; Feng, X.; Mullen, K.; Passerone, D.; Pignedoli, C. A.; Ruffieux, P.; Fasel, R.; Meyer, E. Superlubricity of Graphene Nanoribbons on Gold Surfaces. *Science* **2016**, *351*, 957−961.
(52) Repp, J.; Meyer, G.; Paavilainen, S.; Olsson, F. E.; Persson, M. Imaging Bond Formation between a Gold Atom and Pentacene on an Insulating Surface. *Science* **2006**, *312*, 1196−1199.
(53) Schuler, B.; Fatayer, S.; Mohn, F.; Moll, N.; Pavliček, N.; Meyer, G.; Peña, D.; Gross, L. Reversible Bergman Cyclization by Atomic Manipulation. *Nat. Chem.* **2016**, *8*, 220−224.
(54) Pavliček, N.; Mistry, A.; Majzik, Z.; Moll, N.; Meyer, G.; Fox, D. J.; Gross, L. Synthesis and Characterization of Triangulene. *Nat. Nanotechnol.* **2017**, *12*, 308−311.
(55) Kaiser, K.; Scriven, L. M.; Schulz, F.; Gawel, P.; Gross, L.; Anderson, H. L. An SP-Hybridized Molecular Carbon Allotrope, Cyclo[18]carbon. *Science* **2019**, *365*, 1299−1301.
(56) Kawai, S.; Krejčí, O.; Nishiuchi, T.; Sahara, K.; Kodama, T.; Pawlak, R.; Meyer, E.; Kubo, T.; Foster, A. S. Three-Dimensional Graphene Nanoribbons as a Framework for Molecular Assembly and Local Probe Chemistry. *Sci. Adv.* **2020**, *6*, No. eaay8913.
(57) Kawai, S.; Sang, H.; Kantorovich, L.; Takahashi, K.; Nozaki, K.; Ito, S. An Endergonic Synthesis of Single Sondheimer-Wong Diyne by Local Probe Chemistry. *Angew. Chem.; Int. Ed.* **2020**, *59*, 10842−10847.
(58) Zhong, Q.; Ihle, A.; Ahles, S.; Wegner, H. A.; Schirmeisen, A.; Ebeling, D. Constructing Covalent Organic Nanoarchitectures Molecule by Molecule *via* Scanning Probe Manipulation. *Nat. Chem.* **2021**, *13*, 1133−1139.
(59) Albrecht, F.; Fatayer, S.; Pozo, I.; Tavernelli, I.; Repp, J.; Peña, D.; Gross, L. Selectivity in Single-Molecule Reactions by Tip-Induced Redox Chemistry. *Science* **2022**, *377*, 298−301.
(60) Mohn, F.; Repp, J.; Gross, L.; Meyer, G.; Dyer, M. S.; Persson, M. Reversible Bond Formation in a Gold-Atom−Organic-Molecule Complex as a Molecular Switch. *Phys. Rev. Lett.* **2010**, *105*, No. 266102.
(61) Choi, B.-Y.; Kahng, S.-J.; Kim, S.; Kim, H.; Kim, H. W.; Song, Y. J.; Ihm, J.; Kuk, Y. Conformational Molecular Switch of the Azobenzene Molecule: A Scanning Tunneling Microscopy Study. *Phys. Rev. Lett.* **2006**, *96*, No. 156106.
(62) Ozaki, T. Variationally Optimized Atomic Orbitals for Large-Scale Electronic Structures. *Phys. Rev. B* **2003**, *67*, No. 155108.
(63) Ozaki, T.; Kino, H. Numerical Atomic Basis Orbitals from H to Kr. *Phys. Rev. B* **2004**, *69*, No. 195113.
(64) Ozaki, T.; Kino, H. Efficient Projector Expansion for the *ab initio* LCAO Method. *Phys. Rev. B* **2005**, *72*, No. 045121.
(65) Otero-de-la-Roza, A.; Blanco, M. A.; Martín Pendás, A.; Luaña, V. Critic: a New Program for the Topological Analysis of Solid-State Electron Densities. *Comput. Phys. Commun.* **2009**, *180*, 157.
(66) Otero-de-la-Roza, A.; Johnson, E. R.; Luaña, V. Critic2: A Program for Real-Space Analysis of Quantum Chemical Interactions in Solids. *Comput. Phys. Commun.* **2014**, *185*, 1007.
(67) van der Heijden, N. J.; Hapala, P.; Rombouts, J. A.; van der Lit, J.; Smith, D.; Mutombo, P.; Švec, M.; Jelinek, P.; Swart, I. Characteristic Contrast in Δfmin Maps of Organic Molecules Using Atomic Force Microscopy. *ACS Nano* **2016**, *10*, 8517−8525.

https://doi.org/10.1021/acs.nanolett.5c03477
Nano Lett. 2025, 25, 13040−13046